The solar photospheric nitrogen abundance

Analysis of atomic transitions with 3D and 1D model atmospheres

E. Caffau[1], E. Maiorca[2], P. Bonifacio[3,1,4], R. Faraggiana[5], M. Steffen[6], H.-G. Ludwig[3,1], I. Kamp[7], and M. Busso[2,8]

[1] GEPI, Observatoire de Paris, CNRS, Université Paris Diderot, 92195 Meudon Cedex, France
  e-mail: Elisabetta.Caffau@obspm.fr
[2] Department of Physics, University of Perugia, via Pascoli, 06123 Perugia, Italy
[3] CIFIST Marie Curie Excellence Team, France
[4] Istituto Nazionale di Astrofisica, Osservatorio Astronomico di Trieste, via Tiepolo 11, 34143 Trieste, Italy
[5] Dipartimento di Astronomia, Università degli Studi di Trieste, via G.B. Tiepolo 11, 34143 Trieste, Italy
[6] Astrophysikalisches Institut Potsdam, An der Sternwarte 16, 14482 Potsdam, Germany
[7] Kapteyn Astronomical Institute, Postbus 800, 9700 AV Groningen, The Netherlands
[8] Istituto Nazionale di Fisica Nucleare, section of Perugia, via Pascoli, 06123 Perugia, Italy

ABSTRACT

Context. In recent years, the solar chemical abundances have been studied in considerable detail because of discrepant values of solar metallicity inferred from different indicators, i.e., on the one hand, the "sub-solar" photospheric abundances resulting from spectroscopic chemical composition analyses with the aid of 3D hydrodynamical models of the solar atmosphere, and, on the other hand, the high metallicity inferred by helioseismology.
Aims. After investigating the solar oxygen abundance using a CO^{5}BOLD 3D hydrodynamical solar model in previous work, we undertake a similar approach studying the solar abundance of nitrogen, since this element accounts for a significant fraction of the overall solar metallicity, Z.
Methods. We used a selection of atomic spectral lines to determine the solar nitrogen abundance, relying mainly on equivalent width measurements in the literature. We investigate the influence on the abundance analysis, of both deviations from local thermodynamic equilibrium ("NLTE effects") and photospheric inhomogeneities ("granulation effects").
Results. We recommend use of a solar nitrogen abundance of $A(N) = 7.86 \pm 0.12^\star$, whose error bar reflects the line-to-line scatter.
Conclusions. The solar metallicity implied by the CO^{5}BOLD-based nitrogen and oxygen abundances is in the range $0.0145 \leq Z \leq 0.0167$. This result is a step towards reconciling photospheric abundances with helioseismic constraints on Z. Our most suitable estimates are $Z = 0.0156$ and $Z/X = 0.0213$.

Key words. Sun: abundances – stars: abundances – hydrodynamics – line: formation

1. Introduction

The knowledge of the precise nitrogen abundance in the solar photosphere is important because N accounts for about 6% (by mass) of the solar metallicity, and hence is one of the most important contributors to Z after O (53%), C (23%), and Ne (14%). Amongst others, the value of Z has a crucial impact on stellar structure calculations. The abundance of C, N, and O in the solar system can be determined only from the solar spectrum. Meteoritic samples are un-representative, because C, N, and O are volatile elements. With condensation temperatures of only a few hundred Kelvin, they condense only partially so that their abundances in pristine meteorites (e.g., carbonaceous chondrites) do not provide valid estimates of the average solar system composition. The main molecule formed by C and O, carbon monoxide (CO), is also extremely stable. As a consequence, all C will be locked into CO if the original material is O-rich, and will be unable to form solid compounds. Only the remaining C

may condense into grains, and in the resulting meteoritic sample carbon will be underrepresented. The reverse is true if the environment is C-rich: all oxygen remains in the gas phase and the remaining C may form grains. Therefore, the global elemental C/O ratio cannot be inferred from meteorites; although, isotopic ratios can be measured with high accuracy. Similar problems affect nitrogen in an even more severe manner. As a consequence, the meteoritic C, N, and O abundances are lower than the solar photospheric ones by large factors: 2−3 for oxygen, about 10 for carbon, and more than 40 for nitrogen (see e.g., Palme & Jones 2003). Analyses of observations of the solar corona also do not provide reliable abundance measurements of these elements. Several processes affect the solar corona composition, partially changing the abundance of some elements (Anders & Grevesse 1989; Grevesse & Sauval 2000). The solar nitrogen abundance can be derived reliably only from the photospheric spectrum.

Besides its importance in determining the solar metallicity, nitrogen is an interesting element from a nucleosynthetic point of view. Its main production channel is the CNO cycle, in which it is produced at the expense of C and O. The main astrophysical

---

* $A(N) \equiv \log n(N) - \log n(H) + 12$.

N production sites remain unclear; AGB stars are good candidates, in addition to rotating massive stars. Nitrogen is measured in many different objects: hot stars, cool stars, Galactic and extragalactic H II regions, and Damped Lyα systems at high redshift. For all of these studies, a good solar reference value is of fundamental importance.

The measurements of heavy element abundances inferred from photospheric solar spectra should agree with results from helioseismology. Helioseismology can provide a measurement of the solar metallicity in essentially three ways: i) from the depth of the convection zone: this depends sensitively on the opacity at the base of the convection zone, which in turn is a function of the abundance of heavy elements (Basu & Antia 1997); ii) using information from the core: the small-frequency spacings of low-degree modes and their separation ratios are sensitive to the mean molecular weight in the core, which can be related to the metallicity of the outer layers (Basu et al. 2007); iii) from the sound speed gradient in the ionisation zone: the depth profile of this quantity can be inferred from helioseismic inversions, and comparison with the results of theoretical solar structure models of different metallicity allows us to place tight constraints on Z (Antia & Basu 2006). A comprehensive review on helioseismology and solar abundances is given by Basu & Antia (2008) which the reader is referred to for further details. It is remarkable that all helioseismic methods provide results that are fairly consistent with each other, which infer a higher metallicity than currently deduced from the analysis of the photospheric spectrum.

In this paper, we determine the photospheric nitrogen abundance by using data for atomic lines and the latest CO^5BOLD solar model. One of our aims is to combine this result with our other solar abundance determinations to obtain a measure of the solar Z based on the CO^5BOLD solar model, and to compare this with the Z values inferred by helioseismology.

2. Nitrogen abundance indicators

2.1. Forbidden lines

The strongest forbidden [N I] lines within the ground configuration are close to 1040.0 nm and belong to the multiplet $^2D^0-^2P^0$. Houziaux (1961) claimed to detect these lines in the solar spectrum, although studies by Lambert & Swings (1967) and Swensson (1967) could not confirm these detections. Swensson (1967) also demonstrated convincingly that the predicted equivalent widths are too weak to be detectable in the Jungfraujoch Atlas.

2.2. Permitted lines

The permitted N I lines of low excitation potential occur at UV wavelengths, mostly in the 80−120 nm range. The atomic N I lines measurable in the solar spectrum are found in the visual and near IR range, and all have a high excitation potential ($E_{low} > 10.3$ eV), implying that these lines are formed in the deep layers of the photosphere. They are therefore hardly affected by departures from LTE ($\Delta A(N) \sim -0.05$ dex, Rentzsch-Holm 1996). In the classical analysis that is based on 1D model atmospheres, these lines have the disadvantage of being very sensitive to the temperature structure of the deep layers, which, for theoretical models, depends on the treatment of convection and, most significantly, on the choice of the mixing-length parameter (see Fig. 1). In principle, these difficulties are overcome by
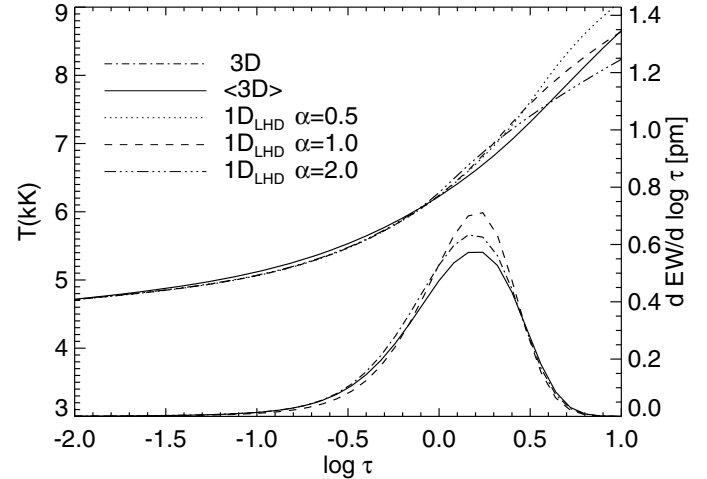

Fig. 1. The temporal and horizontal average of the temperature profile of the 3D model (solid line) and the temperature profile of $1D_{LHD}$ models of three values of α_{MLT}, are shown as a function of (Rosseland) optical depth. In addition, equivalent width contribution functions (lower, roughly Gaussian-shaped curves) for the 746.8 nm line at disc-centre are plotted as a function of monochromatic continuum optical depth.

modern 3D hydrodynamical simulations, which provide a physically consistent description of convection from first principles.

2.3. Molecular lines

Grevesse et al. (1990) illustrated that atomic and molecular lines react in opposite directions to temperature perturbations, so that the agreement between the atomic and molecular lines provides support for the choice of solar model. In their molecular analysis, they and other authors have relied on the use of NH and CN molecular lines. In this paper, we derive the solar N abundance from only the atomic lines and defer the study of molecular lines to the future. On the one hand the abundance of carbon has not yet been estimated with a CO^5BOLD model, and on the other hand, synthesising the NH A-X band, used e.g. by Lambert (1978) in the solar spectrum, would require accounting for a large number of lines, both NH lines and blending atomic lines, and the state-of the art version of Linfor3D is unable to handle hundreds of lines. Potential deviations from LTE for the molecular species is another issue that hampers the use of molecular lines for accurate abundance analysis. For these reasons, we postpone the study of molecular lines harbouring N.

2.4. Line selection

The first selection of lines was completed by extracting all the N I lines from the NIST Atomic Spectra Database (NIST ASD Ralchenko 2005) in the range 400−1200 nm. These lines were then checked by visual inspection in the solar atlases of Delbouille et al. (1973) and Delbouille et al. (1981); the identifications were achieved by using the Utrecht spectrum identifications (Moore et al. 1966) for the 400−877 nm range, and those by Swensson et al. (1970) for the 900−1200 nm range. According to the NIST ASD, no N I line is present in the 877−900 nm range, which is not covered by these identification lists. We also performed a check of the relative line intensities with the Moore Multiplet Table (Moore 1945). The strongest and least blended lines are given in Table 1 with the log gf values, and their qualities taken from the NIST ASD.

Table 1. Selection of permitted N I lines in the visual and near IR spectral range.

λ (nm)	E_{low} (eV)	log gf	Q	n_{low}	n_{up}
744.229	10.330	–0.385	B+	4	10
746.831	10.336	–0.190	B+	4	10
821.634	10.336	+0.132	B+	4	9
822.314	10.330	–0.271	B+	4	9
868.340	10.330	+0.087	B+	4	8
871.883	10.336	–0.336	B+	4	8
1010.513	11.750	+0.219	B+	8	17
1011.248	11.758	+0.607	B+	8	17
1011.464	11.764	+0.768	B+	8	17
1050.700	11.840	+0.094	B	9	20
1052.058	11.840	+0.010	B	9	20
1053.957	11.844	+0.503	B	9	20

Notes: error of log gf ≤ 0.03 dex (Q = B+), ≤0.08 dex (Q = B); n_{low} and n_{up} identify the level of the nitrogen model atom used for the NLTE computations (cf. Fig. 3).

3. Models and line-formation codes

3.1. 3D hydrodynamical model atmosphere

Our analysis is based mainly on a 3-dimensional radiation-hydrodynamics simulation (hereafter 3D model) computed with the CO⁵BOLD code (Freytag et al. 2002, 2003; Wedemeyer et al. 2004). Some basic information about the setup of this numerical simulation can be found in Caffau et al. (2008), who used the same model to determine the solar oxygen abundance. A full description of the model, including a critical review of its performance in reproducing various observational constraints, will be given in Ludwig et al. (2009).

3.2. 1D reference models

For comparison, we also used several 1D solar models:

1. The semi-empirical Holweger-Müller model (Holweger 1967; Holweger & Müller 1974, hereafter HM); when necessary, this was placed on a mass column-density scale, using the opacity used to produce the CO⁵BOLD model.
2. A 1D model computed with the LHD code, which uses the same microphysics as CO⁵BOLD and treats convection with the mixing-length approximation, adopting α_{MLT} = 1.0 (see Caffau & Ludwig 2007, for further details), and two further 1D$_{\text{LHD}}$ models with α_{MLT} of 0.5 and 2.0, to investigate the dependence of the abundance on α_{MLT}.
3. The ATLAS9 solar model with the abundances of Asplund et al. (2005) as computed by Castelli[1].
4. A 1D model obtained by temporal and horizontal averaging over surfaces of equal (Rosseland) optical depth and over all snapshots. We refer to this averaged model as ⟨3D⟩.

3.3. Line-formation calculations

The 3D spectrum synthesis computations are all performed with Linfor3D[2], which can also compute line formation using as input different type of 1D models. For comparison in the case of

---

[1] http://wwwuser.oats.inaf.it/castelli/sun/ ap00t5777g44377k1asp.dat
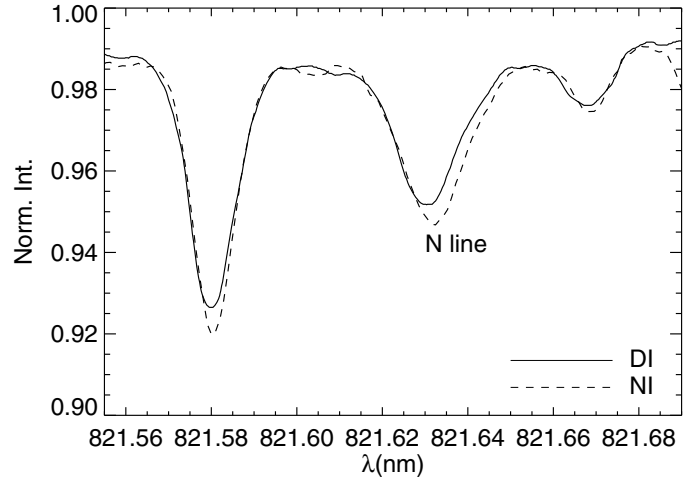[2] http://www.aip.de/~mst/Linfor3D/linfor_3D_manual. pdf

---

Fig. 2. Observed profile of the N I line at λ 821.6 nm as extracted from the Delbouille (solid) and Neckel (dashed) solar disc-centre intensity spectral atlases. The reason for the considerable differences in unknown.

1D models, we also used the SYNTHE code (Kurucz 1993, 2005b) in its Linux version (Sbordone et al. 2004; Sbordone 2005) in calculating synthetic spectra. The advantage of SYNTHE over Linfor3D is that it can easily treat hundreds of thousands of lines, while the present version of Linfor3D is limited to a few tens of lines.

4. Observational data

Investigations of solar abundances found in the literature usually provide detailed discussions about both the accuracy of the adopted model atmospheres and the related uncertainties in the derived abundances. However, the accuracy of the observational data is often not taken into consideration, since, typically, solar abundance determinations rely on a single observed spectrum.

4.1. Differences between high quality solar spectra

In our study of the solar oxygen abundance (Caffau et al. 2008), we noted that different high quality solar spectra exhibit differences that were larger than expected from their high S/N ratios. To investigate the problem related to the differences between the solar atlases in the case of nitrogen, we checked four selected lines. From this non-exhaustive analysis, we conclude, as we did for other elements, that for some, but not all, lines, the solar atlases disagree. This is the case for one of four nitrogen lines that we considered as illustrated in Fig. 2. The presence of telluric absorption might explain this difference. However, by analysing spectra of rapidly rotating hot stars, there is no evidence of any telluric contamination, but the day-time sky can exhibit absorption that is undetectable at night-time. An indisputable reason for the differences still needs to be identified. We strongly believe that the astronomical community needs a new high-quality solar atlas.

4.2. Comparison of different EW measurements

Inspection of the literature often reveals that even the measurement of equivalent widths (*EW*s) from one and the same observed spectrum is less straightforward than what could be expected. Different authors use different approaches and measure different equivalent widths. A recent example is the comparison

of our *EW*s for oxygen (Caffau et al. 2008) with those of Asplund et al. (2004). A long-running debate about the solar iron abundance has in part been driven by differences in the *EW*s (see for example Holweger et al. 1995, and references therein). For the nitrogen, the *EW* measurements differ also between different works. Comparing the measurements of the *EW*s of two authoritative works such as Grevesse et al. (1990) and Biémont et al. (1990), we conclude that there is good agreement for our selected lines of nitrogen. The authors measure similar values without any systematic differences being evident.

4.3. Data used in this study

In our analysis, we used the *EW*s of Grevesse et al. (1990) and Biémont et al. (1990), which are in excellent agreement.

For a few selected lines, we derived in addition the nitrogen abundance from detailed line profile fitting (see Fig. 5). For this purpose, we used the two centre-disc intensity atlases (the "Delbouille" atlas, i.e., Delbouille et al. 1973; Delbouille et al. 1981; and the "Neckel" intensity atlas; Neckel & Labs 1984), as well as the two solar flux atlases (the "Kurucz" solar flux atlas Kurucz 2005a; and the "Neckel" solar flux atlas Neckel & Labs 1984). Further details about these atlases can be found in the aforementioned references and Caffau et al. (2008).

5. NLTE computations

The nitrogen lines considered in our analysis are weak and form deep inside the solar photosphere (see Fig. 1, showing the *EW* contribution function for one of the nitrogen lines). From these facts, we do not expect that these lines are very sensitive to departures from Local Thermodynamic Equilibrium (LTE). In her analysis of the statistical equilibrium of nitrogen in the Sun, Rentzsch-Holm (1996) inferred that the deviations from LTE are small and negative, on average about −0.05 dex. In this paper, we confirm this result.

5.1. 1D NLTE corrections

Since the nitrogen lines form at the same photospheric depth range in both 3D and 1D ($\langle$3D$\rangle$, $1D_{LHD}$) models (see contribution functions in Fig. 1), this infers that 3D granulation effects do not play a fundamental role. Since the contribution functions for 3D and 1D models are similar, it follows that the computed *EW*s are also similar, implying that the 3D corrections are small. Without a code capable of solving the full 3D-NLTE problem for nitrogen, we resort to 1D-NLTE calculations.

We computed the departures from LTE for the $\langle$3D$\rangle$ and HM models, using the Kiel code (Steenbock & Holweger 1984), with the model atom of Rentzsch-Holm (1996). The Kiel code uses a generalisation of the Drawin (1969) formalism to take into account excitation and ionisation of the nitrogen atoms by inelastic collisions with neutral hydrogen atoms. A scaling factor, S_H, permits to reduce the efficiency of these collisions ($S_H < 1$), to switch them off ($S_H = 0$), or to consider them "in toto" ($S_H = 1$). Consistent with the Kiel group and in line with Rentzsch-Holm (1996), we favour $S_H = 1/3$, even though we computed NLTE corrections in addition for $S_H = 0$ and $S_H = 1$. In Fig. 3, the departure coefficients of the atomic levels relevant to the selected lines (see Table 1) are shown for the $\langle$3D$\rangle$ model.

The NLTE corrections obtained from the $\langle$3D$\rangle$ and the HM model are given in Table 4. They are added to the abundances obtained from the LTE analysis based on the 3D and
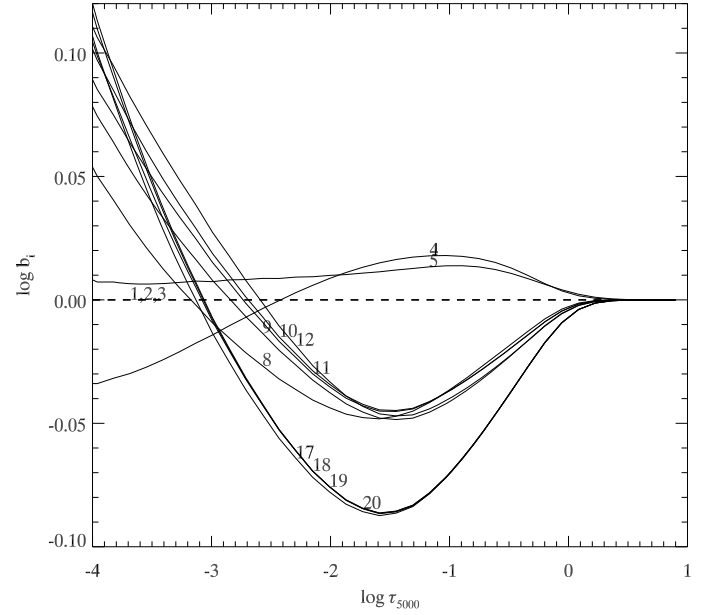
Fig. 3. Departure coefficients $\log b_i = \log(n_{NLTE}/n_{LTE})$ of selected levels of neutral nitrogen as a function of optical depth $\log \tau_{5000}$. For each line involved in our abundance analysis, the identification of the upper and lower level is listed in Table 1. The shown b_i refer to the $\langle$3D$\rangle$ model; similar results are obtained for the HM model.

the HM model, respectively, to obtain the final NLTE nitrogen abundances.

5.2. Influence of horizontal temperature fluctuations

Using the $\langle$3D$\rangle$ model to compute departures from LTE is an extreme case in which all horizontal temperature fluctuations are neglected. To estimate how this approximation affects departures from LTE, we produced horizontal and time-averaged models by grouping columns into twelve bins according to their emergent continuum intensity in the vertical direction. A similar procedure was used by Aufdenberg et al. (2005) to estimate the effects of horizontal, temperature inhomogeneities.

These twelve components represent the different horizontal temperature structures associated with the presence of granules and intergranular lanes. Each component has a weight that depends on its surface area fraction. The cool downdrafts are associated with the groups of lowest intensity, and the warm upflows with those of the highest intensity. We computed NLTE corrections using each of these components, which were treated as standard plane-parallel model atmospheres (1.5D approximation). The components allowed us to study the variations in the NLTE corrections as a function of the temperature structure of the flow where the line is formed. The results, for a selection of lines, are shown in Fig. 4.

Lines with excitation energies higher than 11 eV exhibit little differences in departures from LTE for the twelve group-averaged models. For the lines with lower excitation energies ($E_{low} \approx 10.3$ eV), the groups corresponding to the cool downdrafts (groups 1 to 6) have a correction that is distinctly larger (in absolute value) than for the groups corresponding to the warm upflows (groups 7 to 12). We consider the variation in the NLTE corrections of the various components, relative to the result of the $\langle$3D$\rangle$ model, as an indication of the uncertainty associated with the 1D approximation.

Table 2. $A(N)_{LTE}$ from selected N I lines with EWs from the literature using Linfor3D.

λ (nm)	EW (pm)		$A(N)3D$		$A(N)\langle 3D\rangle$		$A(N)1D_{LHD}$		$A(N)_{HM}$		3D-$\langle 3D\rangle$ dex	3D-1D$_{LHD}(\alpha_{MLT} = 1.0)$ dex
	G	B	G	B	G	B	G	B	G	B		
(1)	(2)	(3)	(4)	(5)	(6)	(7)	(8)	(9)	(10)	(11)	(12)	(13)
744.2	0.26	0.27	7.808	7.826	7.847	7.865	7.810	7.828	7.911	7.928	−0.039	−0.002
746.8	0.52	0.49	7.961	7.931	7.994	7.964	7.954	7.924	8.057	8.027	−0.033	+0.008
821.6	0.86	0.87	7.854	7.860	7.892	7.899	7.847	7.853	7.957	7.963	−0.039	+0.007
822.3	0.24		7.593		7.648		7.611		7.718		−0.055	−0.018
868.3	0.78	0.81	7.828	7.849	7.865	7.885	7.821	7.841	7.929	7.949	−0.037	+0.007
871.8	0.42	0.43	7.927	7.939	7.971	7.983	7.933	7.944	8.036	8.047	−0.044	−0.006
1010.5	0.18		7.956		8.022		7.976		8.098		−0.066	−0.020
1011.2	0.35	0.36	7.897	7.912	7.958	7.971	7.908	7.922	8.033	8.046	−0.060	−0.011
1011.4	0.55	0.54	7.976	7.966	8.028	8.019	7.976	7.967	8.101	8.092	−0.053	−0.001
1050.7	0.14		8.002		8.066		8.022		8.143		−0.064	−0.020
1052.0	0.08		7.829		7.896		7.853		7.975		−0.067	−0.024
1053.9	0.32		7.989		8.046		7.999		8.121		−0.057	−0.010
Average			7.885	7.890	7.936	7.941	7.892	7.897	8.007	8.007	−0.051	−0.008

Notes: columns with G are from Grevesse et al. (1990), with B are from Biémont et al. (1990). Column (1) is the wavelength; Cols. (2), (3) the EWs; Cols. (4)−(11) $A(N)$ from 3D, $\langle 3D\rangle$, 1D$_{LHD}$, and HM model; Cols. (12), (13) two different 3D corrections.

Fig. 4. For five representative lines the 1D-NLTE corrections from the twelve group-averaged models, ordered according to increasing continuum intensity (radiation temperature) from left to right, are shown together with the result for the global $\langle 3D\rangle$ model (rightmost, bold symbol). The lowest curve is plotted at the true ordinate level, while each of the others curves is shifted up by 0.05 dex with respect to the previous one for clarity.

The variations in the NLTE-corrections are small, even for the lower excitation lines, for which the difference between the extreme groups is less than 0.05 dex. We therefore expect that the results we obtained using the $\langle 3D\rangle$ model will not disagree by more than 0.03 dex with the results of a full 3D-NLTE computation.

6. Nitrogen abundance determinations

6.1. LTE abundance from selected lines

The following abundance analysis is based on a subsample of lines given in Table 1. We determined individual LTE nitrogen abundances, $A(N)_{LTE}$ using the 3D, $\langle 3D\rangle$, 1D$_{LHD}$, and HM model, respectively, and the equivalent width measurements by Grevesse et al. (1990) and Biémont et al. (1990) where available. The results are given in Table 2. In this table and in the

others following, we indicate the abundances to three decimal places, following the prescription of Bevington & Robinson (2003) of retaining one more significant digit than dictated by the error. For nitrogen lines, which are formed in the deep photosphere, the 3D correction, defined as $A(N)_{3D}−A(N)_{1D_{LHD}}$, Col. (13), is small, in the range −0.024−0.008 dex. The "granulation abundance correction", $A(N)_{3D}−A(N)_{\langle 3D\rangle}$, (indicated in Col. (12) of Table 2), which measures the influence of horizontal fluctuations, is somewhat larger, and negative for all the lines. We reported similar behaviour for the O I 615.8 nm line in previous work (see Caffau et al. 2008).

6.2. Line-profile fitting

We selected four clean and not too weak lines from the set of lines in Table 1 (746.8 nm, 821.6 nm, 868.3 nm, and 1011.4 nm) for which we fitted the line profile for all the four observed atlases (two fluxes and two centre-disc intensities), using 1D models with SYNTHE as a line formation code. We discarded the line at 1011.4 nm for which we could not obtain a reliable fit; the abundance that we derived from this line was also too high to be consistent with those found for other lines, although we note that the four different spectra consistently indicated the same (high) abundance. The line list used in the profile fitting of this line appears to be incomplete. Nevertheless, we decide to retain this line in the abundance determination inferred from the EWs, because there it is consistent with the other values, indicating that the line decomposition method used to determine EW is reliable.

The $A(N)$ derived from the line at 821.6 nm in the four different spectra exhibits a scatter of 0.050 dex, when considering the $\langle 3D\rangle$-NLTE abundance, which is considerably larger than the scatter found for the other two lines. The difference between the $A(N)$ derived from the two disc-integrated spectra is about 0.06 dex, while the $A(N)$ from the two centre-disc spectra differ by about 0.13 dex. Neither the two disc-integrated spectra nor the two centre-disc spectra do agree (see Fig. 2). The difference in EW is of the order of 15%. This is much larger than expected from the high S/N ratio of the spectra.

The line fitting results are given in Table 3. An example of the excellent agreement achieved in the line fitting using the HM model, is shown in Fig. 5.

Table 3. A(N) of N I from line fitting using 1D models with SYNTHE.

Observed spectrum	λ (nm)	HM	A(N)$_{\mathrm{LTE}}$ ATLAS9	$\langle 3D \rangle$	A(N)$_{\mathrm{NLTE}}$ $\langle 3D \rangle$
KF	746.8	7.861	7.824	7.809	7.750
NF	746.8	7.874	7.837	7.827	7.768
NI	746.8	7.890	7.834	7.823	7.785
DI	746.8	7.908	7.849	7.840	7.802
KF	821.6	7.847	7.811	7.805	7.730
NF	821.6	7.918	7.870	7.867	7.792
NI	821.6	7.944	7.879	7.873	7.821
DI	821.6	7.808	7.752	7.746	7.694
KF	868.3	7.910	7.889	7.857	7.783
NF	868.3	7.906	7.877	7.857	7.783
NI	868.3	7.933	7.878	7.875	7.831
DI	868.3	7.932	7.886	7.882	7.838

Notes: Col. (1) is the observed spectrum identification, KF: Kurucz Flux, NF: Neckel Flux, NI: Neckel Intensity, and DI: Delbouille Intensity; Col. (2) is the wavelength; Cols. (3)−(5) the A(N)$_{\mathrm{LTE}}$ from line fitting with HM, ATLAS9, and $\langle 3D \rangle$ model; Col. (6) is the A(N)$_{\mathrm{NLTE}}$ for the $\langle 3D \rangle$ model, obtained by adding the NLTE-correction computed with $S_{\mathrm{H}} = 1/3$ to the abundances given in Col. (5).
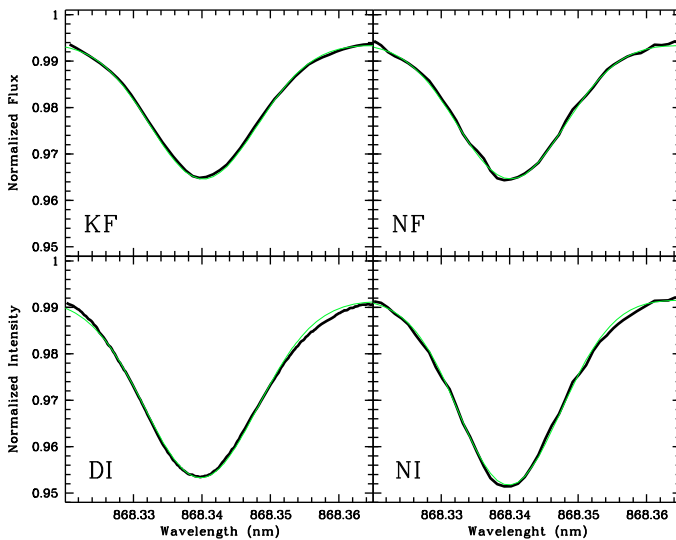
Fig. 5. Results of the line profile fits for the 868.3 nm line. The synthetic spectra computed with SYNTHE and using the Holweger-Müller model (thin lines) are superimposed on the observed spectra from the four solar atlases (KF = Kurucz flux, NF = Neckel Flux, DI = Delbouille Intensity, NI = Neckel Intensity; thick lines).

The differences between the nitrogen abundance from both the fitting procedure and by matching the measured *EW*s can be explained by the influence of blending components, which are accounted for in different ways in the line-fitting approach and in the *EW* method, respectively. The different codes used may also be responsible for part of the difference.

Since the majority of the nitrogen lines are blended, weak, or both, the line-fitting approach is, in principle, more appropriate. However, line fitting with 3D spectra can become a tedious task, and we therefore prefer to rely on equivalent width measurements. We believe that we cannot achieve superior measurement of the *EW*s than the careful works by Grevesse et al. (1990) and Biémont et al. (1990). In principle, we could also measure the *EW*s in data from the other atlases, but our above line fitting exercise implies that this would introduce an additional scatter of the order of at most approximately 0.03 dex, due to the
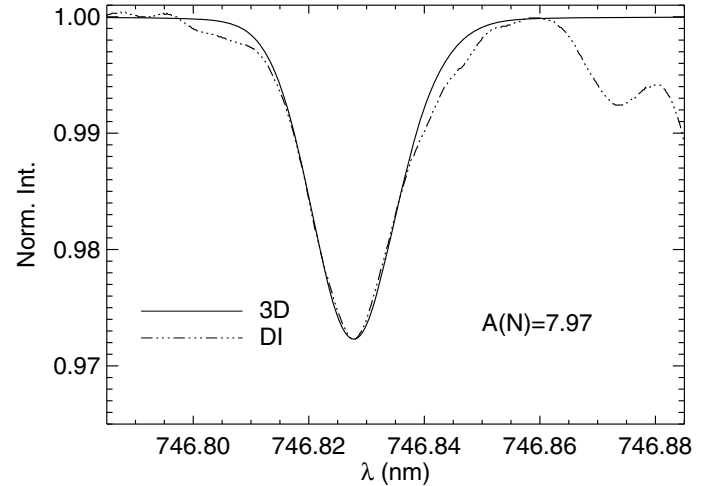

Fig. 6. The unblended 3D profile of N I 746.8 nm is compared to the observed solar centre-disc profile of the Neckel Intensity atlas.

differences between atlases. As we shall see, this is much less than the scatter derived from the different lines. Our final choice is therefore to derive A(N) from the *EW*s from Grevesse et al. (1990) and Biémont et al. (1990), using both 3D and 1D models.

As a consistency check, we also compared the 3D profiles with the observed spectra, as shown for one example in Fig. 6. The agreement is in general good, given that the blending line visible in the observed spectrum were not considered in the synthetic 3D profile.

6.3. 3D-NLTE abundance

Table 4 provides the NLTE corrections for both the $\langle 3D \rangle$ and the HM models. Our final 3D-NLTE nitrogen abundance is obtained by averaging the 12 individual 3D-NLTE abundances (Col. (2) + Col. (4)), with equal weight. The individual as well as the averaged NLTE-corrections are given in Cols. (4)−(6), respectively. The result is:

$$
\begin{aligned}
A(\mathrm{N}) &= 7.85 \pm 0.12 \quad \text{for} \ S_{\mathrm{H}} = 0 \\
A(\mathrm{N}) &= 7.86 \pm 0.12 \quad \text{for} \ S_{\mathrm{H}} = 1/3 \\
A(\mathrm{N}) &= 7.87 \pm 0.12 \quad \text{for} \ S_{\mathrm{H}} = 1.
\end{aligned}
\tag{1}
$$

With the *EW*s from Biémont et al. (1990), A(N) remains the same while the scatter is reduced to 0.06 dex, since the scatter is insensitive to the choice of S_{H} due to these lines being formed at similar depths in the solar photosphere and having similar, and, in any case, small, NLTE corrections.

7. Discussion

7.1. 3D effects and NLTE-corrections

A decisive point in favour of using 3D hydrodynamical models (or a semi-empirical model) is that there is no need to invoke mixing-length theory. All the nitrogen lines used in our abundance determination arise from transitions between levels of high excitation energy, so that they are formed deep in the solar photosphere, in the range $-1 < \log \tau < +1$, and hence are sensitive to the choice of the mixing-length parameter in classical 1D models. A change of $^{+1.0}_{-0.5}$ in the value of the mixing-length parameter of 1.0 that we adopt, produces a change in the abundance with the 1D$_{\mathrm{LHD}}$ model of on average $^{-0.09}_{+0.05}$ dex. The "granulation abundance correction", A(N)$_{\mathrm{3D}} - A$(N)$_{\langle 3D \rangle}$, is

Table 4. $A(N)_{LTE}$ and $\Delta A(N)_{NLTE}$ from selected N I lines with disc-centre *EW*s from the literature obtained with Linfor3D and Kiel code for NLTE computations.

λ (nm)	$A(N)3D_{LTE}$		$\Delta A(N)_{NLTE} \langle 3D\rangle$ S_H			$A(N)HM_{LTE}$		$\Delta A(N)_{NLTE}$ HM S_H		
	G	B	1/3	1	0	G	B	1/3	1	0
(1)	(2)	(3)	(4)	(5)	(6)	(7)	(8)	(9)	(10)	(11)
744.2	7.808	7.826	–0.034	–0.026	–0.038	7.911	7.928	–0.038	–0.028	–0.042
746.8	7.961	7.931	–0.038	–0.030	–0.042	8.056	8.027	–0.043	–0.032	–0.047
821.6	7.854	7.860	–0.052	–0.037	–0.064	7.957	7.963	–0.057	–0.041	–0.071
822.3	7.593		–0.039	–0.028	–0.049	7.718		–0.045	–0.032	–0.056
868.3	7.828	7.849	–0.047	–0.034	–0.061	7.929	7.949	–0.051	–0.036	–0.065
871.8	7.927	7.939	–0.040	–0.029	–0.052	8.036	8.047	–0.044	–0.032	–0.058
1010.4	7.956		–0.017	–0.012	–0.025	8.098		–0.020	–0.015	–0.029
1011.2	7.897	7.912	–0.019	–0.014	–0.028	8.033	8.046	–0.023	–0.016	–0.032
1011.4	7.976	7.966	–0.021	–0.015	–0.039	8.101	8.092	–0.024	–0.017	–0.035
1050.7	8.002		–0.010	–0.007	–0.016	8.143		–0.012	–0.009	–0.020
1052.0	7.829		–0.010	–0.007	–0.017	7.975		–0.011	–0.008	–0.018
1053.9	7.989		–0.011	–0.009	–0.018	8.121		–0.013	–0.009	–0.022
Average	7.885	7.890	–0.028	–0.020	–0.037	8.007	8.007	–0.032	–0.023	–0.041

Notes: columns with G are from Grevesse et al. (1990), with B are from Biémont et al. (1990). Column (1) is the wavelength; Cols. (2), (3) $A(N)$ from 3D model, Cols. (4)−(6) the corresponding NLTE corrections for $S_H = 1/3,\ 1,\ 0$, respectively; Cols. (7), (8) $A(N)$ from HM model; Cols. (9)−(11) the corresponding NLTE corrections for $S_H = 1/3,\ 1,\ 0$, respectively.

always negative, ≈ -0.05 dex on average, in agreement with the results of Steffen & Holweger (2002). The total 3D correction, defined as $A(N)_{3D} - A(N)_{1D_{LHD}}(\alpha_{MLT} = 1.0)$ is only slightly negative for most of the considered lines. Therefore, the 3D model provides a slightly smaller abundance (by ≈ -0.01 dex) than the $1D_{LHD}$ model.

The NLTE effects for the analysed lines are small and negative, so that $A(N)_{LTE} > A(N)_{NLTE}$. The average NLTE correction, for $S_H = 1/3$, is about -0.03 dex.

7.2. Estimating the solar metallicity

Our favoured values for the solar nitrogen abundance, $A(N) = 7.86$, and the solar oxygen abundance, $A(O) = 8.76$ (Caffau et al. 2008), imply a revision of the solar metallicity Z. The two other elements important to the determination of the solar metallicity (in terms of fractional mass) are neon and carbon.

Neon is not measurable in the spectrum of the solar photosphere. The usual procedure is to measure the ratio Ne/O in the solar corona, and assume this value to be the same as in the photosphere. We may consider Ne/O = 0.15 (Asplund et al. 2005) or Ne/O = 0.18 (Grevesse & Sauval 1998), implying $A(Ne) = 7.94$ and $A(Ne) = 8.02$, respectively. By studying Ne abundances in nearby B-type stars Morel & Butler (2008) found a mean $A(Ne) = 7.97 \pm 0.07$, and suggest that this value should also be representative of the solar Ne abundance. Wang & Liu (2008) pointed out that the Ne/O ratios in H II regions and planetary nebulae equal on average 0.25, and suggested that the current estimate of the solar Ne/O ratio could be too low. If the solar Ne/O ratio was so large, the Ne abundance would be 8.16. We may therefore consider four possible values of $A(Ne)$, ranging from 7.94 to 8.16. For the carbon abundance, we have three choices, $A(C) = 8.52$ according to Grevesse & Sauval (1998), $A(C) = 8.39$ from Asplund et al. (2005), or $A(C) = 8.592$ from Holweger (2001).

The situation is summarised in Table 5, where our $A(N)$ and $A(O)$ are used with all possible combinations of $A(Ne)$ and $A(C)$ to provide Z and Z/X. The metallicity Z spans the range 0.0146 to 0.0167, while Z/X spans the range 0.0199 to 0.0228. All these values are considerably higher than the values recommended by

Table 5. Solar metallicity (Z and Z/X) for different choices of C and Ne abundance.

$A(C)$	8.39	8.52	8.59
$A(Ne)$		$Z; Z/X$	
7.94	0.0146; 0.0199	0.0153; 0.0209	0.0158; 0.0216
7.97	0.0146; 0.0199	0.0154; 0.0210	0.0159; 0.0218
8.02	0.0148; 0.0202	**0.0156; 0.0213**	0.0161; 0.0220
8.16	0.0154; 0.0210	0.0162; 0.0221	0.0167; 0.0228

Asplund et al. (2005) ($Z = 0.0122$ and $Z/X = 0.0165$), and the increase is mainly driven by our higher oxygen abundance, although the adopted values of N, C, and Ne also play a role.

7.3. Metallicity from helioseismology

This upward revision alleviates the tension between photospheric abundances and helioseismic data, and the two may essentially agree. Using the solar *relative* composition of Asplund et al. (2005) and OP opacities, Basu & Antia (2008) inferred from the depth of the convection zone that $Z/X = 0.0218 \pm 0.0008$, although the computation should be repeated with our solar composition, but we note that this value is already within the range of the Z/X in Table 5. Using the Asplund et al. (2005) solar composition and one of their test models, Chaplin et al. (2007) derived $Z = 0.0161 \pm 0.00008$ from low-degree modes, again in the range of values of Table 5. Using the more extensive set of models obtained from a Monte Carlo simulation, Chaplin et al. (2007) inferred values of between $Z = 0.0187$ and $Z = 0.0239$. These values are definitely higher than any of the values in Table 5. From the solar sound-speed profile, Antia & Basu (2006) derive $Z = 0.0172 \pm 0.002$. Again, this value is higher than any value in Table 5, even though it is within 2σ of the highest value in the table.

8. Conclusions

Our recommended value of the solar nitrogen abundance is $A(N) = 7.86 \pm 0.12$, which takes into account 3D effects and deviations from LTE. This value is between the value inferred by

Asplund et al. (2005) (7.78 ± 0.06) and that found by Grevesse & Sauval (1998) (7.92 ± 0.06). Our A(N) is slightly lower, although consistent within errors, with the result found by Holweger (2001, A(N) = 7.931 ± 0.111).

In the course of our analysis, we found considerable differences between the various solar spectral atlases, introducing additional uncertainties in the abundances derived from individual lines. The disagreement is by far larger than what can be attributed to the noise in the spectra. This fact has been pointed out already in our previous solar abundance studies. We believe that the quality of the available solar spectral atlases, which date back 30 or more years, should be improved by making use of up-to-date technology.

Our most robust estimate of the solar Z is obtained by adopting the abundances of Grevesse & Sauval (1998) for all elements except for oxygen, nitrogen, and neon, for which we take our own abundances, A(O) = 8.76, A(N) = 7, 86, and A(Ne) = 8.02. The latter results from the ratio Ne/O = 0.18 given by Grevesse & Sauval (1998), combined with our oxygen abundance. In this way, the resulting solar metallicity is Z = 0.0156 and Z/X = 0.0213, respectively.

Pending a new determination of the solar C abundance, we can say that our new results for N and O represent a significant step in forward reconciling photospheric abundances with helioseismic constraints on Z.

References

Anders, E., & Grevesse, N. 1989, Geochim. Cosmochim. Acta, 53, 197
Antia, H. M., & Basu, S. 2006, ApJ, 644, 1292
Asplund, M., Grevesse, N., Sauval, A. J., Allende Prieto, C., & Kiselman, D. 2004, A&A, 417, 751
Asplund, M., Grevesse, N., & Sauval, A. J. 2005, Cosmic Abundances as Records of Stellar Evolution and Nucleosynthesis, ASP Conf. Ser., 336, 25
Aufdenberg, J. P., Ludwig, H.-G., & Kervella, P. 2005, ApJ, 633, 424
Basu, S., & Antia, H. M. 1997, MNRAS, 287, 189
Basu, S., & Antia, H. M. 2008, Phys. Rep., 457, 217
Basu, S., Chaplin, W. J., Elsworth, Y., et al. 2007, ApJ, 655, 660
Bevington, P. R., & Robinson, D. K. 2003, Data reduction and error analysis for the physical sciences, 3rd edn., ed. P. R. Bevington, & K. D. Robinson (Boston, MA: McGraw-Hill)
Biémont, E., Froese Fischer, C., Godefroid, M., Vaeck, N., & Hibbert, A. 1990, 3rd International Colloquium of the Royal Netherlands Academy of Arts and Sciences, 59

Caffau, E., & Ludwig, H.-G. 2007, A&A, 467, L11
Caffau, E., Ludwig, H.-G., Steffen, M., et al. 2008, A&A, 488, 1031
Chaplin, W. J., Serenelli, A. M., Basu, S., et al. 2007, ApJ, 670, 872
Delbouille, L., Roland, G., & Neven, L. 1973, Liege: Universite de Liege, Institut d'Astrophysique
Delbouille, L., Roland, G., Brault, J. W., & Testerman, L. 1981, Photometric atlas of the solar spectrum from 1850 to 10 000 cm^{-1}, http://bass2000.obspm.fr/solar_spect.php
Drawin, H. W. 1969, Z. Physik, 225, 483
Freytag, B., Steffen, M., & Dorch, B. 2002, Astron. Nachr., 323, 213
Freytag, B., Steffen, M., Wedemeyer-Böhm, S., & Ludwig, H.-G. 2003, CO5BOLD User Manual, http://www.astro.uu.se/~bf/co5bold_main.html
Grevesse, N., & Sauval, A. J. 1998, Space Sci. Rev., 85, 161
Grevesse, N., & Sauval, A. J. 2000, Origin of Elements in the Solar System, Implications of Post-1957 Observations, 261
Grevesse, N., Lambert, D. L., Sauval, A. J., et al. 1990, A&A, 232, 225
Holweger, H. 1967, ZAp, 65, 365
Holweger, H. 2001, Joint SOHO/ACE workshop, Solar and Galactic Composition, AIP Conf. Proc., 598, 23
Holweger, H., & Müller, E. A. 1974, Sol. Phys., 39, 19
Holweger, H., Kock, M., & Bard, A. 1995, A&A, 296, 233
Houziaux, L. 1961, Zeitschrift fur Astrophysik, 53, 237
Kurucz, R. 1993, SYNTHE Spectrum Synthesis Programs and Line Data. Kurucz CD-ROM No. 18 (Cambridge, Mass.: Smithsonian Astrophysical Observatory)
Kurucz, R. L. 2005a, Mem. Soc. Astron. Ital. Suppl., 8, 189
Kurucz, R. L. 2005b, Mem. Soc. Astron. Ital. Suppl., 8, 14
Lambert, D. L. 1978, MNRAS, 182, 249
Lambert, D. L., & Swings, J. P. 1967, The Observatory, 87, 113
Ludwig, H.-G., Steffen, M., Freytag, B., et al. 2009, A&A, in preparation
Moore, C. E. 1945, Contributions from the Princeton University Observatory, 20, 1
Moore, C. E., Minnaert, M. G. J., & Houtgast, J. 1966, National Bureau of Standards Monograph (Washington: US Government Printing Office (USGPO))
Morel, T., & Butler, K. 2008 [arXiv:0806.0491]
Mugglestone, D. 1958, MNRAS, 118, 432
Neckel, H., & Labs, D. 1984, Sol. Phys., 90, 205
Palme, H., & Jones, A. 2003, Meteorites, Comets and Planets: Treatise on Geochemistry, 1, 41
Ralchenko, Y. 2005, Mem. Soc. Astron. Ital. Suppl., 8, 96, http://physics.nist.gov/PhysRefData/ASD/index.html
Rentzsch-Holm, I. 1996, A&A, 305, 275
Sbordone, L. 2005, Mem. Soc. Astron. Ital. Suppl., 8, 61
Sbordone, L., Bonifacio, P., Castelli, F., & Kurucz, R. L. 2004, Mem. Soc. Astron. Ital. Suppl., 5, 93
Steenbock, W., & Holweger, H. 1984, A&A, 130, 319
Steffen, M., & Holweger, H. 2002, A&A, 387, 258
Swensson, J. W. 1967, Zeitschrift fur Astrophysik, 66, 156
Swensson, J. W., Benedict, W. S., Delbouille, L., & Roland, G. 1970, Mémoires of the Société Royale des Sciences de Liège, 5
Wang, W., & Liu, X. 2008, MNRAS, in press [arXiv:0806.2288]
Wedemeyer, S., Freytag, B., Steffen, M., Ludwig, H.-G., & Holweger, H. 2004, A&A, 414, 1121